Research Article

SURFACE and INTERFACE ANALYSIS

Received: 30 July 2009 Revised: 1 December 2009 Accepted: 2 December 2009 Published online in Wiley Interscience:

(www.interscience.wiley.com) DOI 10.1002/sia.3183

Effect of heat treatment on the properties and structure of TiO_2 nanotubes: phase composition and chemical composition

D. Regonini,[a] A. Jaroenworaluck,[b] R. Stevens[a]* and C.R. Bowen[a]

Titanium oxide (TiO_2) nanotubes prepared by electrolytic anodisation of a titanium electrode have been systematically heat treated to control the conversion of the as-prepared amorphous structure to nanocrystalline anatase and rutile. Raman spectroscopy revealed that the temperature of calcination is critical in determining the structure and crystallinity of the titania. X-ray Photoelectron Spectroscopy analysis shows the as-prepared film to consist mainly of oxide, although a small amount of fluoride contamination remains from the electrolyte. Organic components from post-anodising cleaning treatments were also present. Fluorine ions are gradually ejected from the anodic layer during annealing and the fluorine concentration is negligible in samples that are heat treated above 400 °C. Choosing the appropriate annealing temperature allows the structure to be made up of defined proportions of anatase and rutile with a reduced contamination of species from the electrolyte or organic solvents. **Copyright © 2010 John Wiley & Sons, Ltd.**

Keywords: titanium oxide; nanotubes; calcination; phase change

Introduction

Previous publications[1–3] have shown the growth of titania (TiO_2) nanotubes on titanium can lead to a controlled length and consistent product of nanotubes aligned perpendicular to the plane of the electrode. The structure of the titania membrane is that of a honeycomb made up of an amorphous titania film with extremely fine regions of crystallinity.[4] The nanotubes are vertical to the electrode surface and are generally arranged in a hexagonal array.[5] The diameter of the nanotubes can be controlled to some extent by the use of different electrolytes and anodisation potentials.[6] Such structures offer considerable potential in chemical reaction control and also in photochemistry, a major potential application being in dye-sensitised photocells.[7–9] For these applications, although the macrostructure can be controlled (tube length, diameter, etc.), the nanostructure and crystalline state of the nanotube is of considerable significance because the efficiency of many chemical and physical reactions can be optimised by the development of the anatase or rutile crystalline phases.[10,11]

This paper explores the development of phase structure and chemical composition of the films during calcination (annealing) of the anodised titania at a constant temperature. In [new additional ref 12], we will characterise the development of the fine-scale structure of the films using electron microscopy and the key nano-features of the crystalline phases.

Experimental Techniques

A commercially pure (99.6%) titanium sheet (0.5 mm thick) was used as an electrode/substrate to be anodised. To complete the cell, a platinum mesh was placed at the cathode to act as a counter-electrode. Prior to anodising, the titanium was ultrasonically cleaned in isopropyl alcohol. Anodising was performed under potentiostatic conditions, applying a voltage within the range 10–60 V. The electrolyte was slightly stirred during the experiment and both a water-based electrolyte and organic-based electrolyte was used to control the length of the tubes. The electrolyte type and temperature (20 °C) were maintained constant for all the experiments.

After anodisation, the nanotube films were annealed in air, at 200, 300, 400, 500, 550 and 600 °C for the nanotubes grown in aqueous NaF/Na_2SO_4 and at 450 and 500 °C for the nanotubes grown in glycerol.

In this paper, characterisation of the as-prepared and annealed specimens was undertaken using Raman spectroscopy and X-ray photoelectron spectroscopy (XPS). Raman analysis was undertaken using a Renishaw RM2000 Laser Raman Spectroscopy instrument to detect the phases which are formed at a specific annealing temperature. A helium-neon laser (632.8 nm) was used as a source of a monochromatic light, calibrated to the silicon peak at 520 cm^{-1}. The machine was fitted with an optical microscope with a laser spot less than 2 μm in diameter. Analyses were performed within the range 300–700 cm^{-1}, which allows discrimination between anatase and rutile, both of which were expected to be found in annealed samples. Data were processed using a freeware spectroscopy software Spekwin 32 programme.

The chemical composition of the as-prepared and annealed layers was characterised using XPS to observe how the chemical content of the anodic oxide changes with the thermal treatment.

* *Correspondence to: R. Stevens, Materials Research Centre, Department of Mechanical Engineering, University of Bath, Claverton Down Road, Bath BA2 7AY, UK. E-mail: r.stevens@bath.ac.uk*

a *Materials Research Centre, Department of Mechanical Engineering, University of Bath, Claverton Down Road, Bath BA2 7AY, UK*

b *MTEC, 114, Pahlyothin Rd., Pathumthani 12120, Thailand*

 Copyright © 2010 John Wiley & Sons, Ltd.

Table 1. Conditions used for surface and depth profiling XPS analysis of anodised TiO_2 films

	Anode filament	Passing energy	Scanned (analysed) area	Etching conditions
Surface analysis	10 keV, 10 mA, 100 W	40–160 eV	300 × 700 μm^2	–
Depth profiling	10 keV, 10 mA, 100 W	40 eV	A spot of 110 μm in diameter	Ar at 4 keV (15 mA); raster 1.5 mm; four etching cycles (45 s per cycle)

This is particularly relevant in order to determine if annealing can reduce or eliminate possible nanotube contaminants such as fluorine (from the electrolyte) and carbon (from organics used during cleaning). XPS analysis was undertaken using a Kratos Axis Ultra-DLD system. The instrument had both a monochromated X-ray source (Al) and a dual Al–Mg anode, and the spectrometer was equipped with a delay-line detector (DLD). The Kratos XPS has a fast chamber for loading the samples (it can be vacuumed down at typically 10^{-8} to 5×10^{-9} torr by means of a turbopump), a preparation chamber (turbopump, 10^{-9} torr) and the analysis chamber (turbopump + ion pump, 5×10^{-10} torr). Conditions adopted during XPS measurements are summarised in Table 1. Using the monochromated Al source, the surface composition of as-prepared and annealed specimens (fixed on a holder using a conductive carbon tape to minimise positive charging) has been studied. Depth profiling analysis has also been performed using an Ar^+ ion sputtering gun operating at 4 keV and 15 mA, to evaluate the changes in water content and impurities, through the thickness of the anodic layer. As a result of the Ar beam and the particles removed by etching, the pressure registered in the analysis chamber during depth profiling measurements was 3×10^{-8} torr. Data analysis and processing was undertaken using the computer-aided software analysis for X-ray photoelectron spectroscopy (CASA XPS).

In [new additional ref 12], X-ray diffraction (XRD) has been used to follow the crystallisation of the titania film during heat treatment to provide a useful comparison with the Raman technique. Morphological and microstructural changes promoted by annealing will be discussed on the basis of both scanning electron microscopy (SEM) and transmission electron microscopy (TEM). High-resolution TEM (HRTEM) has also been used to support the Raman observations and to determine the crystal phase of the titanium dioxide present after the heat treatment.

Results and Discussion

Thermal treatment on anodised TiO_2 nanotubes

Previous studies[4,13] have indicated that as-prepared nanotubes develop as an amorphous gel of hydroxylated TiO_2 (especially when anodising in water-based electrolytes), sometimes containing very small crystals of anatase. It is of interest to establish how the anodic layer changes following a post-thermal treatment, which is required to convert the as-prepared amorphous layer into a fully crystalline material. Several applications are envisaged for the films of fully crystalline nanotubes, including dye-sensitised solar cells and as a catalytic support for redox and photochemical reactions. For such applications, the particular phase present, its purity and even the particle size can have an influence on the efficiency of the processes as a result of the change in band-gap energy measured with different crystallographic phases.[1] The most comprehensive work on annealed anodised titania nanotubes has been published by Grimes and co-workers in 2003[2]; they demonstrated that nanotubes are stable up to 580 °C when annealed in an ambient oxygen atmosphere. At a higher annealing temperature, the crystallisation of the titanium substrate disturbed the tubular architecture causing collapse and sintering of the structure. They observed rutile protrusions emerging from the metal structure at a high temperature (500 °C or higher) and identified the protrusions as the main reason for the collapse of the nanotubes. Owing to a size constraint they also observed the crystal structure within the tubes remained as anatase. The anatase to rutile transformation in the tubes could be attained using a humid argon atmosphere, forming rutile nanotubes without collapse of the structure, this being accompanied by shrinkage of the porous network. Limited work has been done on the effect of the annealing since Grimes investigated relatively short (500 nm length) nanotubes.[2] In this work, the effect of thermal treatment on anodic TiO_2 nanotubes layers having a thickness of 1.6 μm (grown in a water-based electrolyte) and 4–5 μm (grown in an organic-based electrolyte) is reported. Figure 1 shows the initial structure of as-prepared nanotubes grown in the water-based (Fig. 1a) and organic-based (Fig. 1b) electrolytes.

Raman spectroscopy of annealed TiO_2 nanotubes

A first evaluation of the phase changes taking place during annealing has been made using Raman spectroscopy, which allows the signals from the oxide grown on the metallic substrate to be optimised. Owing to its metallic nature, titanium has free electrons preventing the lattice vibrations and it is therefore not an active contributor to Raman. Analysis was undertaken in the range 300–700 cm^{-1}, the optimum region for discriminating between the different crystal phases of TiO_2.[3,14,15] Signals from anatase and rutile have been observed within the temperature range examined (from as-prepared to samples annealed up to 600 °C). Brookite, by far the less common crystal phase of titanium dioxide, which would also have had characteristic peaks within the 300–700 cm^{-1} region has not been detected in any of the samples. The spectra recorded for the specimens anodised in aqueous Na_2SO_4/NaF and annealed at different temperatures are shown in Fig. 2.

Raman peaks are not present at 200 °C, indicating the amorphous nature of the sample; the spectra start to change at 300 °C with the appearance of anatase peaks (A in Fig. 2) at approximately 400 cm^{-1} (corresponding to the B_{1g} vibration mode), 520 cm^{-1} (A_{1g} mode) and 640 cm^{-1} (E_g mode). Anatase signals persist throughout the entire range of annealing temperatures, and become more intense with each increase in temperature. From the Raman data, it would appear that a minimum temperature of 300 °C is necessary to induce crystallisation of the anodic film although, in Part II, TEM investigation on as-prepared samples has revealed the presence of small crystalline islands before any thermal treatment.[4] It is possible that the crystals in the as-prepared samples are too small in size or, more likely, are in

Copyright © 2010 John Wiley & Sons, Ltd.

SURFACE and INTERFACE ANALYSIS

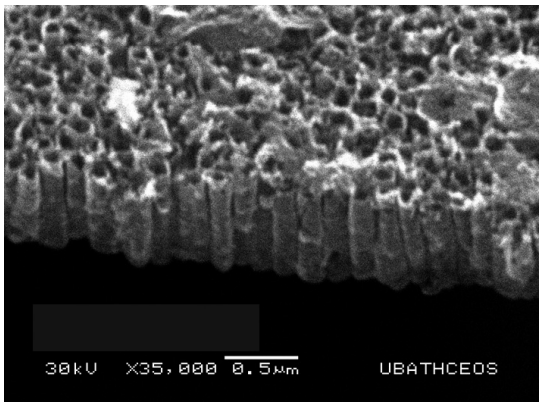

(a)

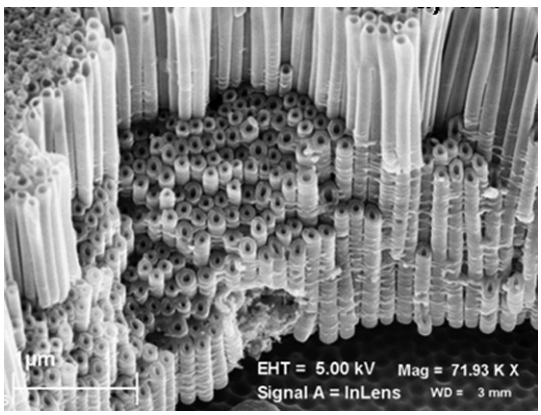

(b)

Figure 1. Typical structure of as-prepared nanotubes grown using (a) aqueous NaF/Na_2SO_4 and (b) NaF/glycerol-based electrolytes.

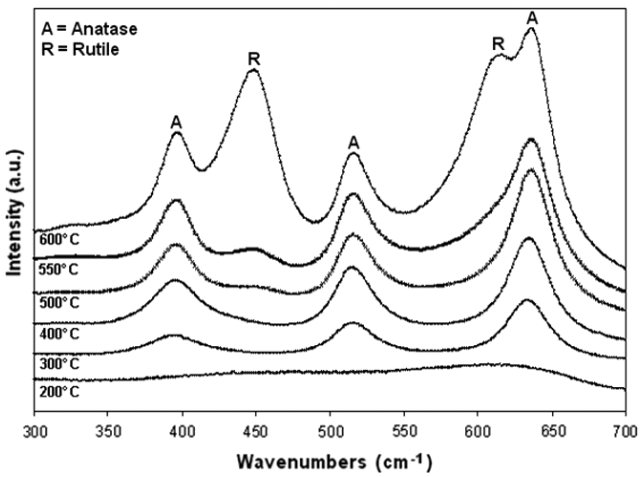

Figure 2. Raman spectroscopy showing crystal phase changes in anodised titania nanotubes prepared in aqueous NaF/Na_2SO_4 electrolyte, and annealed in air at different temperatures, from 200 to 600 °C.

insufficient quantity within the amorphous matrix and this does not allow their detection by means of Raman. Furthermore, from Raman spectroscopy, in addition to anatase, the presence of a second phase, rutile, is also detected after annealing at 500 °C and at higher annealing temperatures. The rutile phase (R in Fig. 2) first appears in samples annealed at 500 °C with a peak occurring

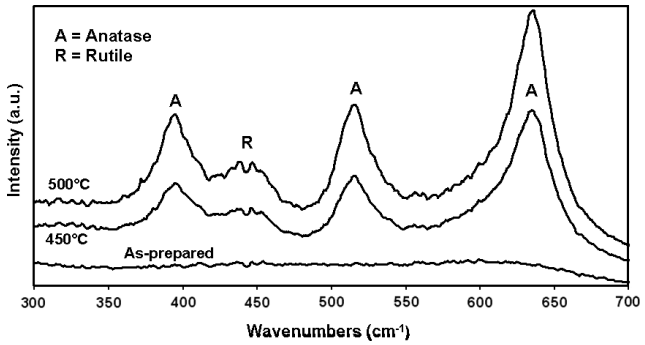

Figure 3. Raman spectroscopy showing crystal phase changes in anodised titania nanotubes prepared in a NaF/glycerol electrolyte, as-prepared, and annealed at 450 or 500 °C.

at approximately 450 cm^{-1} (E_g mode). Rutile also has a second characteristic peak at approximately 615 cm^{-1} (A_{1g} mode) which is clearly visible at 600 °C as a shoulder of the anatase signal at 640 cm^{-1}, whereas it is hidden by the latter at 500 and 550 °C, since rutile is just starting to form and its intensity is lower. Peak values are in good agreement with those previously reported for TiO_2 nanoparticles.[16] Owing to the nanosize scale of the tubes, along with bulk mode vibrations, there are the so-called interfacial vibrations (i.e. due to the fact most of the material is at the surface) which broaden the peaks and shifts them to slightly lower wavelengths.[17–19]

Similar conclusions can be drawn for the nanotube samples grown in a NaF/glycerol electrolyte, where the nanotubes are normally longer (4–5 µm compared with 1.6 µm for those prepared in water) and have a smaller diameter than tubes grown in water-based media. Raman spectra of specimens anodised using the organic electrolyte and annealed at different temperatures (450 and 500 °C), as well as of an as-prepared sample are shown in Fig. 3. The information provided by the Raman spectra are similar to that observed for samples grown in an aqueous electrolyte. Again the as-prepared film is amorphous and no Raman peaks are observed. On the basis of the conclusions drawn from thermal treatment on TiO_2 films grown in an aqueous electrolyte, the temperature range of 450–500 °C is considered optimum for the development of the anatase phase, which is preferred in photo-voltaic applications, since it leads to a better percolation of electrons and higher photocurrents.[20,21] The dominant phase at 450 and 500 °C is indeed anatase; however, the presence of small rutile peaks at 450 °C suggests that it is better to anneal the specimens at an even lower temperature (300–400 °C) to obtain only anatase.

XPS analysis of as-prepared TiO_2 tubes grown in aqueous Na_2SO_4/NaF

The chemical composition of as-prepared films grown in aqueous Na_2SO_4/NaF media has been studied by XPS. For semi-quantitative analysis, the spectra background (arising from energy loss processes occurring as the photoelectrons are ejected from the specimen) has been subtracted using a Shirley type algorithm. Overlapping peaks (oxygen peak, O 1s) have been resolved in their components by a curve fitting procedure using Gaussian/Lorentzian product functions to delineate the line shape of the different contributions. The choice of a Shirley algorithm was driven by the fact they are specifically thought to allow the use of

 Copyright © 2010 John Wiley & Sons, Ltd.

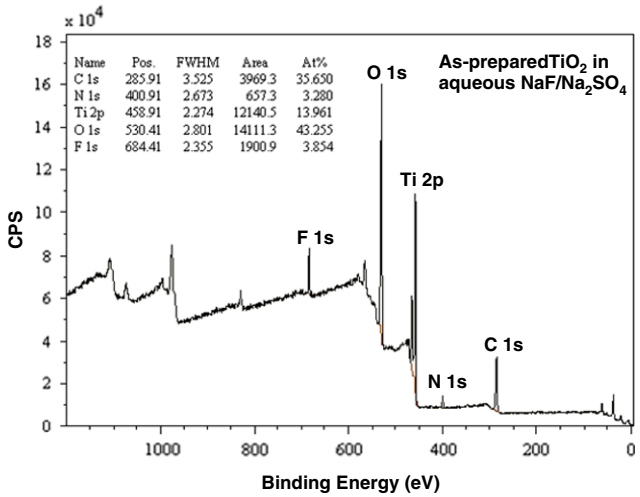

Figure 4. XPS spectra of an as-prepared anodised TiO_2 film grown in an aqueous media. The oxide layer contains a certain degree of impurities, particularly fluoride ions, as expected, plus nitrogen and carbon which are probably related to contamination/adsorption occurring after the electrochemical process.

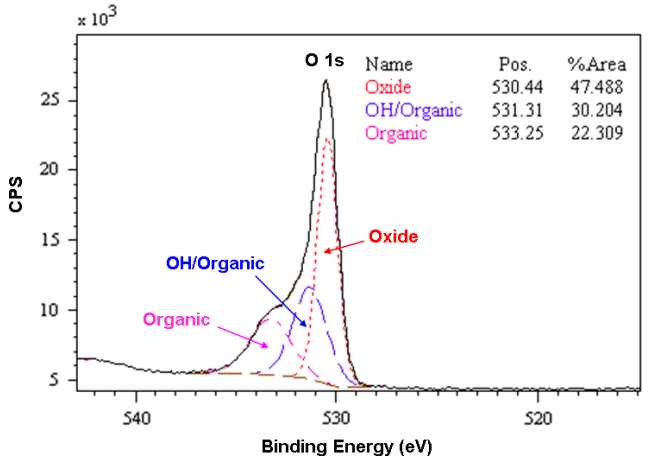

Figure 5. The O 1s signal at 530.4 eV typical of oxygen in TiO_2. The peak also contains two additional components in addition to the oxide, which can be identified as the hydration of the oxide and an organic contamination due to the ultrasonic cleaning in isopropanol.

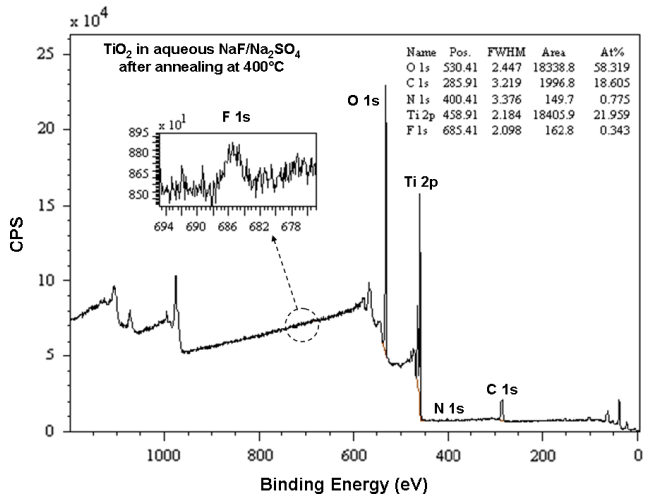

Figure 6. XPS spectra of anodised titania nanotubes grown in aqueous Na_2SO_4/NaF and annealed in air at 400 °C. In terms of chemical composition, the main differences from as-prepared samples are the lower nitrogen, carbon and fluorine content, the latter highlighted in the inset of the image.

a symmetric model to determine the intensity of different components of a peak. The work published by Carley *et al.*[22] provides a general overview on the resolution of overlapping XPS peaks and approaches available.

A typical XPS spectrum registered (at a passing energy of 160 eV) for an as-prepared anodic layer grown in NaF/Na_2SO_4 aqueous solution at 20 V for 10 min. is shown in Fig. 4. An initial voltage ramp of 100 mV s^{-1} was applied to set the voltage at its final anodising value of 20 V, as these were identified as the final standard conditions that lead to the best films in terms of final film thicknesses.[15] However, identical results were also obtained when applying a constant voltage without the use of any voltage ramp, and the discussion is therefore limited to the latter case. The anodic film consists of titanium (Ti 2p), oxygen (O 1s), carbon (C 1s), fluoride (F 1s) and also a small content of nitrogen (N 1s). Occasionally, very small quantities (1 at.%) of silica (contamination from mechanical polishing) and sulfur (from the electrolyte) are detected. The N 1s at 400 eV is due to a small amount of contaminants from the distilled water used for the experiments (also sodium sulfate contained some nitrogen) and possibly to adsorption of nitrogen from the atmosphere.

The significant and unexpected content of carbon (C 1s at 285 eV) has been associated with the post-cleaning process in isopropyl alcohol (which has been used to remove any post-anodising contamination), forming a polymer-like layer by bonding to the oxide. Fluoride contamination (F 1s at 684 eV) from the electrolyte is also presented on the surface of the sample, at an atomic concentration of approximately 3.8 at.%. A more accurate scan (at a passing energy of 40 eV) focused on regions of interest provides further details about the chemical composition of the anodic structure. The formation of titanium dioxide is confirmed by the peaks at 459.1 and 464.8 eV, respectively, due to Ti 2p (3/2) and Ti 2p (1/2), Fig. 5, as well as the O 1s peak at 530.4 eV, Fig. 6, which are characteristic of Ti and O in TiO_2.[23,24] Furthermore, from Fig. 5, it is possible to identify a shoulder in the Ti 2p (3/2) peak at 459.1 eV. The asymmetry is due to the presence of the hexafluorotitanate complex TiF_6^{2-}. The binding energy of the electrons involved in TiF_6^{2-} is higher than in TiO_2, because of the remarkable electronegativity of fluorine.

However, the titanium to oxygen ratio (Ti : O) which emerges from the general results in Fig. 4 is not 1 : 2 as expected for TiO_2, but is approximately 1 : 3. The O 1s signal is in fact the result of three different contributions which are specified in Fig. 5 as the oxygen due to the titanium oxide (530.4 eV), a certain degree of hydration in the oxide, due to a signal typical of a hydroxylic (OH) group (and probably some organic contaminants) at 531.4 eV,[25] and a final component, which is identified as of organic nature at 533.1 eV. The latter is related to the anomalous carbon content in the film and could be the result of the oxygen from isopropanol bonding with the outer oxide layer. Although it is difficult to derive a precise quantitative conclusions from overlapping signals, from a curve fitting analysis of the O 1s signal (i.e. total oxygen in the film), it is possible to estimate the weight of any single contribution. The O 1s peak is approximately the result of a 50% contribution

Copyright © 2010 John Wiley & Sons, Ltd.

from oxygen in the oxide (O_{OXIDE} in Fig. 5), while the remnant parts are due to oxygen from water/hydrated species and from organic origin and are named, respectively, as ($O_{OH/ORGANIC}$) and ($O_{ORGANIC}$), as it is not possible to separate clearly between the organic contribution in the two of them. By accounting the O_{OXIDE} plus $O_{OH/ORGANIC}$ area and neglecting the $O_{ORGANIC}$ component, the ratio Ti : O decreases to approximately 1 : 2.4, which is still an overestimation (due to overlapping), but provides a more realistic composition of the film. The high Ti : O ratio suggests that the oxide film is not purely TiO_2, but it is hydrated when working in water-based media.

A detailed scan on the fluoride peak region (F 1s) allows identification of the signal at 684.9 eV due to the presence of hexafluorotitanate complex TiF_6^{2-}[26] combined with sodium (Na) from the electrolyte, which forms during the anodisation, rather than 'free' fluoride ions, which would give a signal at a slightly lower energy (683–684 eV).[27] This indicates that fluoride ions from the electrolyte rapidly dissolve the oxide as they are incorporated in the film as hexafluorititanate species only. There were no major differences in XPS response for the anodic films formed in glycerol compared with the data from samples formed in aqueous electrolyte.

XPS analysis of annealed TiO_2 tubes grown in aqueous Na_2SO_4/NaF

It is of interest to determine the composition changes of the nanotube film following annealing at different temperatures. The analysis here has been limited to nanotubes grown in aqueous Na_2SO_4/NaF and annealed at 300, 400 and 550 °C. XPS spectra of a sample annealed at 400 °C are shown in Fig. 6. A comparison is made with the spectra obtained for as-prepared samples since the as-prepared film has a strong fluoride signal (Fig. 4) due to contamination of the oxide film from the electrolyte. Figure 6 indicates a large reduction of the fluoride concentration after annealing, highlighted in the inset of the figure. This suggests that fluorine ions, specifically the TiF_6^{2-} species, are expelled from the anodic film during the annealing process at 400 °C and above.

In terms of overall chemical composition, the main differences between the as-prepared and annealed samples are the much lower nitrogen, carbon and fluorine content; compare Figs 4 and 6. This could be used as an advantage in potential applications of nanotubes since a fluorine-rich outer layer represents a problem for the adsorption of a dye on the surface of the oxide when used in sensitised solar cells. The presence of fluorine could also alter the properties of the surface in catalysis, gas sensing and biomedical devices. The decrease of fluorine content following the heat treatment of the film is proportional to the annealing temperature. This can be clearly observed in Fig. 7, where it is shown how the fluorine concentration gradually decreases from 3.8 at.% in as-prepared TiO_2 to 1.0 at.% following heat treatment at 300 °C, 0.3 at.% at 400 °C and finally to a concentration below the detection limit at 550 °C.

Oxygen peaks were examined to assess contamination by organic species which are generally used in cleaning the nanotubes. XPS analysis of the oxygen peaks on the sample annealed at 400 °C before etching with Ar ions (i.e. depth profiling) is shown in Fig. 8a, with the inset representing the situation observed before the heat treatment. It is of interest to observe that the 'organic peak' at 534 eV has almost disappeared, suggesting that some of the contamination introduced by the

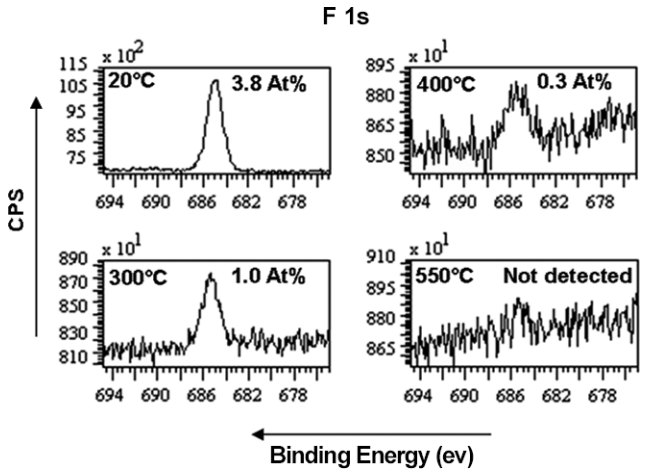

Figure 7. XPS analysis of the fluorine content in anodised TiO_2 nanotubes grown in aqueous Na_2SO_4/NaF and annealed at different temperatures.

cleaning procedure using isopropyl alcohol can be removed by annealing. However, there is still a certain amount of $O_{OH/ORGANIC}$ at 531.7 eV. It is reasonable to assume that the annealed films do not contain any residual hydration (apart from moisture adsorbed after the thermal treatment), and this extra oxygen is again of an organic origin. The composition remains almost identical after etching away the first few superficial layers, as shown in Fig. 8b.

Conclusions

The investigation of thermal treatment on the crystallinity and composition of the anodic TiO_2 nanotubes has shown a number of changes take place during annealing of the as-prepared film in the temperature range 200–600 °C.

(i) Raman spectral analysis shows that it is possible to convert nanotubes prepared in water-based and organic-based electrolytes from amorphous to crystalline anatase and the conversion takes place at approximately 300 °C.
(ii) At a higher annealing temperature, rutile appears (500–550 °C) and becomes the dominant phase (at 600 °C).
(iii) XPS analysis shows the as-prepared film to consist mainly of oxide, with a certain amount of fluoride contamination remaining from the electrolyte. Organic components from post-anodising cleaning treatments are also present.
(iv) XPS analysis indicates that fluorine ions are gradually released from the anodic layer following annealing, and the fluorine concentration is negligible in samples heated at temperatures above 400 °C.
(v) XPS analysis indicated annealed samples have a much lower nitrogen, carbon and organic content compared with as-prepared films.
(vi) Choosing the appropriate annealing temperature allows the phase structure to consist of defined proportions of anatase and rutile with a much reduced contamination from chemical species in the electrolyte or organic solvents.

Acknowledgements

The authors acknowledge Prof. Geoff Allen of the Interface Research Centre at the University of Bristol for use of Raman

Copyright © 2010 John Wiley & Sons, Ltd.

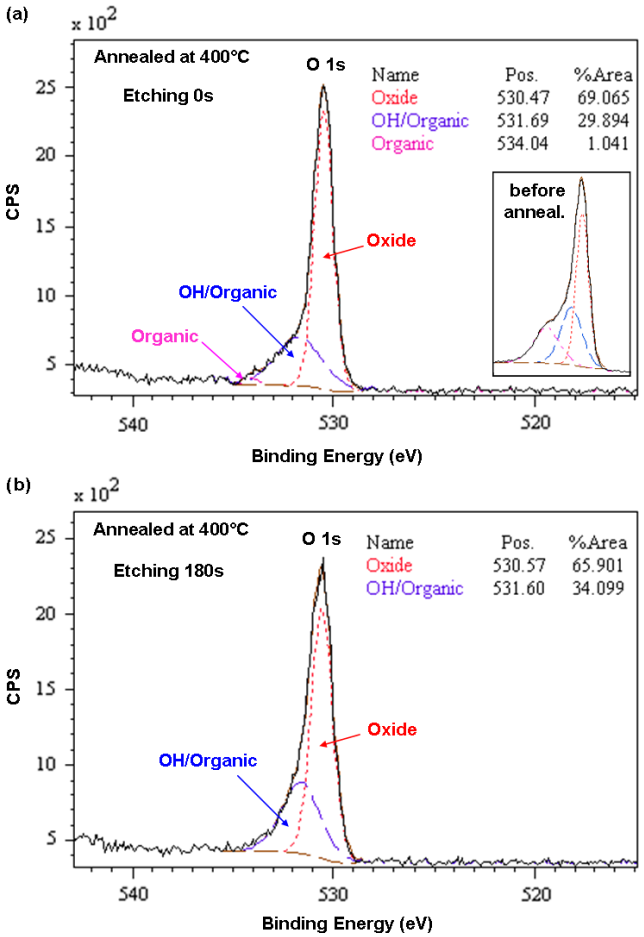

Figure 8. XPS analysis of the oxygen content on a sample anodised TiO_2 nanotubes grown in aqueous Na_2SO_4/NaF and annealed at 400 °C before (a) and after(b) the etching treatment. For comparison, the oxygen peak on an as-prepared sample is reported in the inset of the image (a).

facilities. Cardiff University are also acknowledged for the use of XPS, made available using EPSRC grant EP/F019823/1: 'Access to Materials Research Equipment – Cardiff XPS'.

References

[1] J.-G. Li, T. Ishigaki, X. Sun, *J. Phys. Chem. C* **2007**, *111*, 4969.
[2] O. K. Varghese, D. Gong, M. Paulose, C. A. Grimes, E. C. Dickey, *J. Mater. Res.* **2003**, *18*, 156.
[3] V. C. Farmer, *The Infrared Spectra of Minerals*, Mineralogical Society: London, **1975**.
[4] A. Jaroenworaluck, D. Regonini, C. R. Bowen, R. Stevens, *J. Mat. Res.* **2008**, *23*, 2116.
[5] K. Wang, M. Wei, M. A. Morris, H. Zhu, J. D. Holmes, *Adv. Mat.* **2007**, *19*, 3016.
[6] Q. Cai, M. Paulose, O. K. Varghese, C. A. Grimes, *J. Mater. Res.* **2005**, *20*, 230.
[7] M. A. Fox, M. T. Dulay, *Chem. Rev.* **1993**, *93*, 341.
[8] A. Fujishima, K. Honda, *Nature* **1972**, *238*, 37.
[9] B. O'Regan, M. Grätzel, *Nature* **1991**, *353*, 737.
[10] H. Tang, K. Prasad, R. Sanjines, P. E. Schmid, F. Levi, *J. Appl. Phys.* **1994**, *75*, 2042.
[11] N.-G. Park, J. Van de Lagemaat, A. J. Frank, *J. Phys. Chem. B* **2000**, *104*, 8989.
[12] A. Jaroenworaluck, D. Regonini, C. R. Bowen, R. Stevens, *A microscopy study of the effect of heat treatment on the structure and properties of anodised TiO_2 nanotubes*, *Appl. Surf. Sci.* **2009**, doi:10.1016/j.apsusc.2009.09.078.
[13] A. Jaroenworaluck, D. Regonini, C. R. Bowen, R. Stevens, D. Allsopp, *J. Mat. Sci.* **2007**, *42*, 6729.
[14] G. A. Tompsett, G. A. Bowmaker, R. P. Cooney, J. B. Metson, K. A. Rodgers, J. M. Seakins, *J. Raman Spectrosc.* **1995**, *26*, 57.
[15] D. Regonini, C. R. Bowen, R. Stevens, D. Allsopp, A. Jaroenworaluck, *Physica Status Solidi (A)* **2007**, *204*, 1814.
[16] W. Ma, Z. Lu, M. Zhang, *Appl. Phys. A* **1998**, *66*, 621.
[17] C. A. Melendres, A. Narayanasamy, V. A. Maroni, R. W. Siegel, *J. Mater. Res.* **1989**, *4*, 1246.
[18] H. Cheng, J. Ma, Z. Zhao, L. Qi, *Chem. Mater.* **1995**, *7*, 663.
[19] W. F. Zhang, Y. L. He, M. S. Zhang, Z. Yin, Q. Chen, *J. Phys. D: Appl. Phys.* **2000**, *33*, 912.
[20] H. Tang, K. Prasad, R. Sanjines, P. E. Schmid, F. Levi, *J. Appl. Phys.* **1994**, *75*, 2042.
[21] N.-G. Park, J. Van de Lagemaat, A. J. Frank, *J. Phys. Chem. B* **2000**, *104*, 8989.
[22] A. F. Carley, P. R. Chalker, J. C. Riviere, M. W. Roberts, *J. Chem. Soc. Faraday Trans.* **1987**, *1*, 351.
[23] S. O. Saied, J. L. Sullivan, T. Choudhury, C. G. Pearce, *Vacuum* **1988**, *38*, 917.
[24] D. Gonbeau, C. Guimon, G. Pfister-Guillouzo, A. Levasseur, G. Meunier, R. Dormoy, *Surf. Sci.* **1991**, *254*, 81.
[25] Y. Z. Huang, D. J. Blackwood, *Electrochim Acta* **2005**, *51*, 1099.
[26] D. Briggs, *Handbook of X-ray and Ultraviolet Photoelectron Spectroscopy*, Heyden & Son Ltd.: London, **1977**.
[27] V. I. Nefedov, Y. V. Salyin, G. Leonhardt, R. Scheibe, *J. Electron Spectrosc. Relat. Phenom.* **1977**, *10*, 121.

Copyright © 2010 John Wiley & Sons, Ltd.